RADIO SCIENCE, VOL. 38, NO. 3, 1060, doi:10.1029/2002RS002603, 2003

Determination of plasmaspheric electron density profile by a stochastic approach

Y. Goto, Y. Kasahara,[1] and T. Sato

Department of Communications and Computer Engineering, Kyoto University, Kyoto, Japan

Received 17 January 2002; revised 10 December 2002; accepted 19 February 2003; published 19 June 2003.

[1] The determination of plasmaspheric electron density profiles has been attempted using a stochastic approach, using Omega signals observed on the Akebono satellite. Since the wave normal directions and delay times of Omega signals can be theoretically calculated by ray tracing under an appropriate electron density model, the density profile can be estimated by fitting the calculated directions and times to the observed values. In the present paper, we introduce a flexible model and a novel algorithm in the fitting method, taking into account the stochastic factors of the density distribution and wave propagation. The stochastic representations of directions and times enable us to separately estimate the effects of the ionosphere and the plasmasphere. The validity of the proposed method is examined using observational data collected during the recovery phase of a magnetic storm. In another example, an estimation of the asymmetry of the plasmasphere is attempted. *INDEX TERMS:* 6984 Radio Science: Waves in plasma; 6969 Radio Science: Remote sensing; 2768 Magnetospheric Physics: Plasmasphere; 6982 Radio Science: Tomography and imaging; *KEYWORDS:* electron density profile, satellite observation, VLF wave

Citation: Goto, Y., Y. Kasahara, and T. Sato, Determination of plasmaspheric electron density profile by a stochastic approach, *Radio Sci., 38*(3), 1060, doi:10.1029/2002RS002603, 2003.

1. Introduction

[2] The electron density profile around the Earth has been gradually revealed by direct satellite observations and ground-based measurements of radio waves propagating from the ground due to lightning, naturally induced ULF waves, and waves from GPS (Global Positioning System) satellites. GPS signals enable us to measure the total electron content (TEC), which gives the integrated electron density along the ray path from the satellite to the ground [e.g., *Davies and Hartmann*, 1997; *Mannucci et al.*, 1998]. TEC derived from such radio waves predominantly reflects the electron density in the ionosphere. It is difficult to measure the density profile in the magnetosphere using this technique. For the magnetosphere, the electron density is ordinarily obtained by direct observations from satellites. A single satellite, however, only enables us to probe the in situ electron density along its trajectory. Theoretical studies have investigated the feasibility of using multisatellite radio tomography to determine the electron density profile over large regions of the magnetosphere [*Ergun et al.*, 2000; *Ganguly et al.*, 2000]. These methods require several measurements of group delay and Faraday rotation of radio waves propagating between spacecraft, and the imaged region can be several Earth radii in extent. As a practical demonstration of radio tomography in the magnetosphere, experiments measuring the parameters of wave propagation between satellites have been attempted as part of the mission of the IMAGE satellite using the Radio Plasma Imager (RPI) [*Reinisch et al.*, 2001] as the transmitter. Recently, *Cummer et al.* [2001] reported a successful example of the measurement of wave propagation parameters between the IMAGE and WIND satellites, and demonstrated the feasibility of the magnetospheric radio remote sensing technique.

[3] *Kimura et al.* [1996, 1997, 2001] developed a remote sensing technique for estimationg the electron density profile over a large region of the plasmasphere using data observed onboard the Akebono satellite. In this method, Omega signals of around 10kHz, which had been used for global navigation until 1997, were used. The Omega signals were transmitted from the stations distributed over the world and were continuously detected by the VLF instruments [*Kimura et al.*, 1990] onboard Akebono in the plasmasphere. The wave normal directions and propagation delay times of the Omega signals along the satellite trajectory can be determined from the observed wave data, which can also be calculated by ray tracing. Thus the electron density

[1]Now at Department of Information and Systems Engineering, Kanazawa University, Kanazawa, Japan.

0048-6604/03/2002RS002603$11.00

profile is reconstructed by fitting the calculated wave normal directions and delay times to the observed values. The advantage of this method is that the electron density profile over large regions of the plasmasphere can be estimated with a fine time resolution (~1 hour) using single satellite observations.

[4] For theoretical modeling of the plasmaspheric profile, many sophisticated models have been developed and applied to a variety of problems. SUPIM [*Bailey et al.*, 1996] is one such sophisticated models. In SUPIM the time-dependent equations of continuity, momentum, and energy balance that describe the chemical and physical processes of the Earth's ionosphere and plasmasphere are solved along geomagnetic field lines. In contrast, the diffusive equilibrium model [*Angerami and Thomas*, 1964], in which the plasma in the plasmasphere is assumed to result from ionospheric evaporation, is well-known as the simplest representation of the plasma distribution. *Kimura et al.* [1997] evaluated the degree of fit of their analytical density model, based on the diffusive equilibrium to SUPIM, by giving the model adequate parameters. They reported that the degree of fit of the electron density was quite satisfactory within ±40° geomagnetic latitude, and that their model was flexible enough to simulate the SUPIM electron density, although the temperature finally obtained from their model was not always reliable.

[5] *Goto et al.* [2002] proposed a flexible density model based on the diffusive equilibrium using stochastic differential equations and an appropriate algorithm based on the model fitting framework proposed by *Kimura et al.* [1996]. In the present paper, we apply this method to the data observed on Akebono. In Section 2, after briefly describing the developed model and the fitting algorithm, we introduce a technique to separate the effects of the ionosphere and the plasmasphere to the wave normal directions and delay times of the Omega signals. In Section 3, we show some examples of the application of the developed method. At first, we apply it to a series of observational data during the recovery phase of a magnetic storm. Secondly, we demonstrate that the difference in electron density profile in the northern and southern hemispheres can be derived. In Section 4, we summarize the results and discuss the validity of the method.

2. Methodology

2.1. Density Model and Algorithm

[6] In this subsection, we explain the electron density model and the parameter fitting algorithm proposed by *Goto et al.* [2002]. The electron density N_e along the geomagnetic field line is assumed to be represented by

$$N_e(L, s) = N_0(L) \cdot N_{DE}(s), \quad (1)$$

where N_0 is the electron density at the reference altitude (500km) depending on the L-value, and N_{DE} indicates the decrement ratio of the electron density at the field aligned distance s. For N_{DE}, a diffusive equilibrium-type function is adopted which depends on the relative ion concentrations η_m and the ion temperature at the reference altitude, and the parameter n_T [*Strangeways*, 1986] relates to the temperature gradient with altitude.

[7] In order to represent the global electron density profile, values for N_0 and the parameters η_m and n_T are required. Equation (1) shows that the electron density at the reference altitude, N_0, can be derived from the observed electron density along the satellite trajectory when the appropriate parameters η_m and n_T are given. Since the observed electron density generally includes not only significant variations but also local fluctuations and observational noise, it is necessary to distinguish them and eliminate the latter. In the proposed model, the electron density at the reference altitude, N_0, was assumed to vary with an appropriate smoothness. That is, the electron density at successive points satisfies the following stochastic differential equation:

$$\nabla^2 N_0 \sim N(0, \tau_N^2 \sigma_N^2), \quad (2)$$

where $N(0, \tau_N^2\sigma_N^2)$ represents a Gaussian distribution with a mean of zero and a variance of $\tau_N^2\sigma_N^2$. τ_N^2, is the smoothing parameter which controls the smoothness of N_0, and σ_N^2 is the variance of the observational error of the electron density. By this assumption, N_0 can be calculated from the observed electron density. In order to represent the smoothness of the temperature at the reference altitude, the smoothing parameter τ_T^2 was also defined. Consequently, the necessary parameter to be determined in the model are η_m, n_T, τ_N^2 and τ_T^2.

[8] The parameter set $\Lambda = [n_T, \eta_m, \tau_N^2, \tau_T^2]$ in the density model is determined based on the Bayesian approach [*Akaike*, 1980] as follows. The wave normal directions and delay times of the Omega signals along the satellite trajectory can be determined from the observed wave data. It is well-known that these propagation characteristics can also be calculated by ray tracing under an appropriate density model. Then, the best parameter set, Λ_{opt}, in the density model is evaluated by the goodness-of-fit between the observed and the calculated wave normal directions and propagation delay times. Since the ray paths do not always propagate along a geomagnetic field line, the density distribution at the reference altitude is extrapolated based on equation (2), in order to reconstruct the field-aligned distribution where the satellite does not traverse.

[9] In the Bayesian approach, the index for the evaluation of ABIC [*Akaike*, 1980] is used. ABIC is defined as the minus log-likelihood of the product distribution of the likelihood of the observation and the probability density distribution calculated by ray tracing

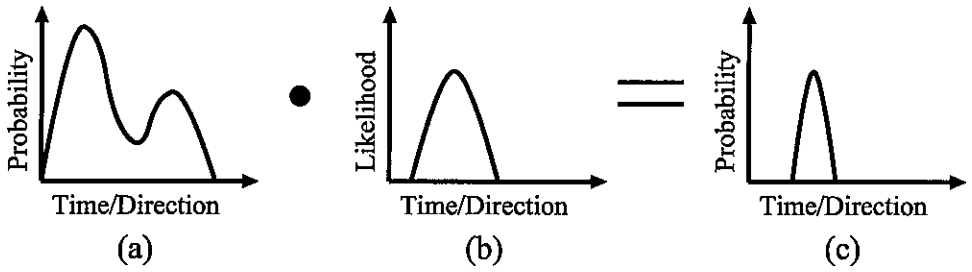

Figure 1. (a) Theoretical distribution obtained by ray tracing, (b) observation including observational errors, and (c) product distribution.

[*Goto et al.*, 2002], as schematically shown in Figure 1. As the volume of the product distribution corresponds to the fit between the calculated and the observed wave characteristics, the best parameter set, Λ_{opt}, can be obtained by finding the minimum ABIC. In the present study, the probability density function (PDF) of the observational error was assumed to be represented by a Gaussian distribution with a mean of zero. The variances of the observational errors were assumed to be 10° for the wave normal direction and 20msec for the delay time. The PDFs of the wave characteristics calculated by ray tracing are constructed by superposing the result of the ray tracing under a variety of initial positions and initial directions. The flowchart for obtaining ABIC from a parameter set Λ is shown in Figure 2. In order to obtain the minimum ABIC, the parameters in Λ are discretized and all combinations of the discretized parameters are examined. A remarkable advantage of this evaluation is that PDFs can represent a variety of possibilities of wave normal directions and delay times, while the former evaluation, based on nonlinear least squares, allows only one theoretical value at an observation point. Thus, the ambiguities of the result of ray tracing can be taken into consideration.

[10] In this algorithm, it should be noted that any electron density model can be used if it has sufficient degrees of freedom to represent the electron density distribution. In the present study, we apply the above-mentioned diffusive equilibrium-type model because it was already confirmed by *Kimura et al.* [1997] that the model is flexible enough to simulate the SUPIM electron density, which is one of the more sophisticated density models.

2.2. Estimation of the Effect of Ionosphere

[11] In the present study, ray tracing was initiated from an altitude of 500km in the region from an L-value of 2 to 4 in order to separate the effects of the ionosphere and the plasmasphere to the wave normal directions and delay times. Due to this separation, it is not necessary to consider the ionospheric profile in the density model, that is, we can calculate the wave normal directions and delay times in the plasmasphere by ray tracing giving adequate initial values at an altitude of 500km.

[12] The wave normal directions of the Omega signals become vertical at the peak altitude of the F2 layer (200–450km) in the ionosphere because the refractive index for the Omega frequencies becomes much larger than unity at the F2 peak. The wave normal direction at an altitude of 500km depends on the altitude of the F2 peak and the electron density profile from the F2 peak

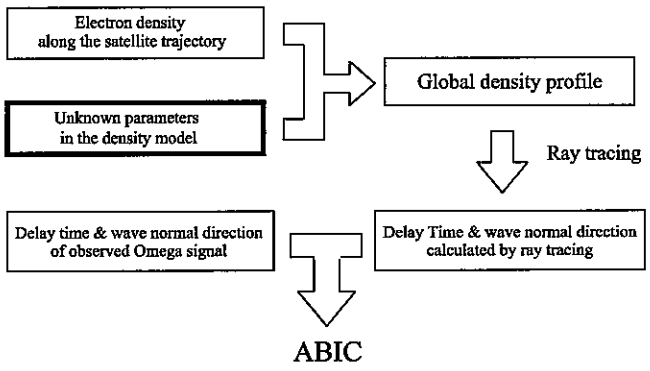

Figure 2. Flowchart to obtain ABIC from a parameter set.

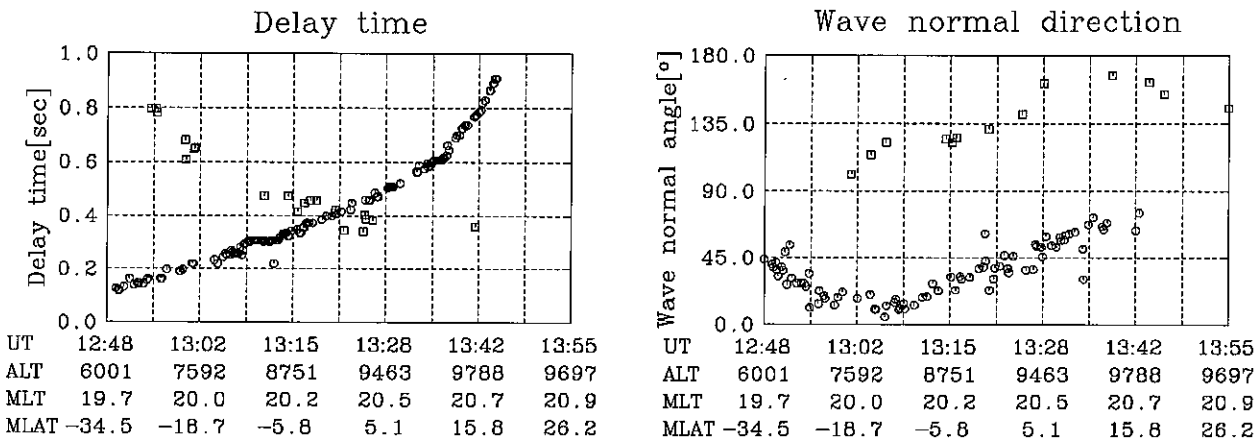

Figure 3. Delay times and wave normal directions of the Omega signal along the trajectory of Akebono on 4 July 1990; the signals from Australia and Japan are indicated by circles and boxes, respectively.

to 500km. *Scarabucci* [1969] derived a numerical formula of the time derivative of the wave normal direction of the VLF wave around the Earth. Based on this formula, the wave normal directions of the Omega signals from both Japan and Australia are inclined toward the magnetic equator in the meridian plane. In the present study, we gave 30 initial directions whose zenith angles are set on from 10° to 50° for each initial position of ray tracing.

[13] As for the delay time in the ionosphere, we estimated it by the international reference ionosphere (IRI) model [*Bilitza et al.*, 1993] and added it to the result of ray tracing. The delay time of the Omega signal in the ionosphere is practically represented as the following integral equation, which is derived from Appleton-Hartree's dispersion equation, along the ray path:

$$t \sim \frac{1}{2c}\int \frac{f_p}{(ff_c\cos\theta)^{\frac{1}{2}}}\,ds, \tag{3}$$

where c is the velocity of light, f_c and f_p are the electron cyclotron frequency and electron plasma frequency, respectively, θ is the angle between the wave normal direction and the geomagnetic field direction, and f is the frequency of the Omega signal. The plasma frequency f_p is proportional to the square root of the electron density. Thus, the total delay time in the ionosphere is essentially proportional to the integral of the square root of the electron density along the ray path.

[14] In the present study, the delay time calculated from the IRI-derived vertical density profiles is 20msec–

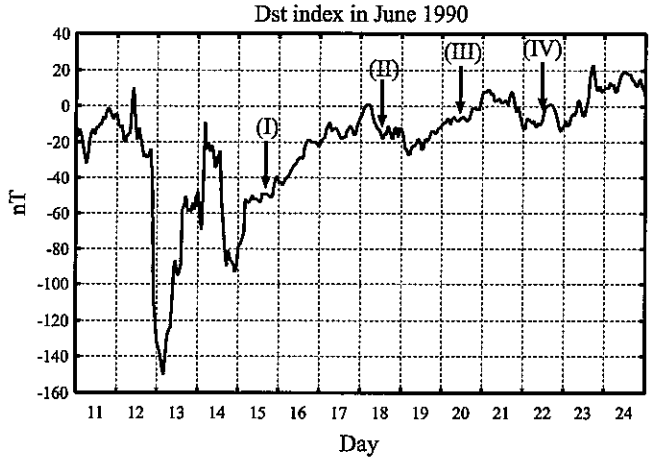

Figure 4. *Dst* index in June 1990.

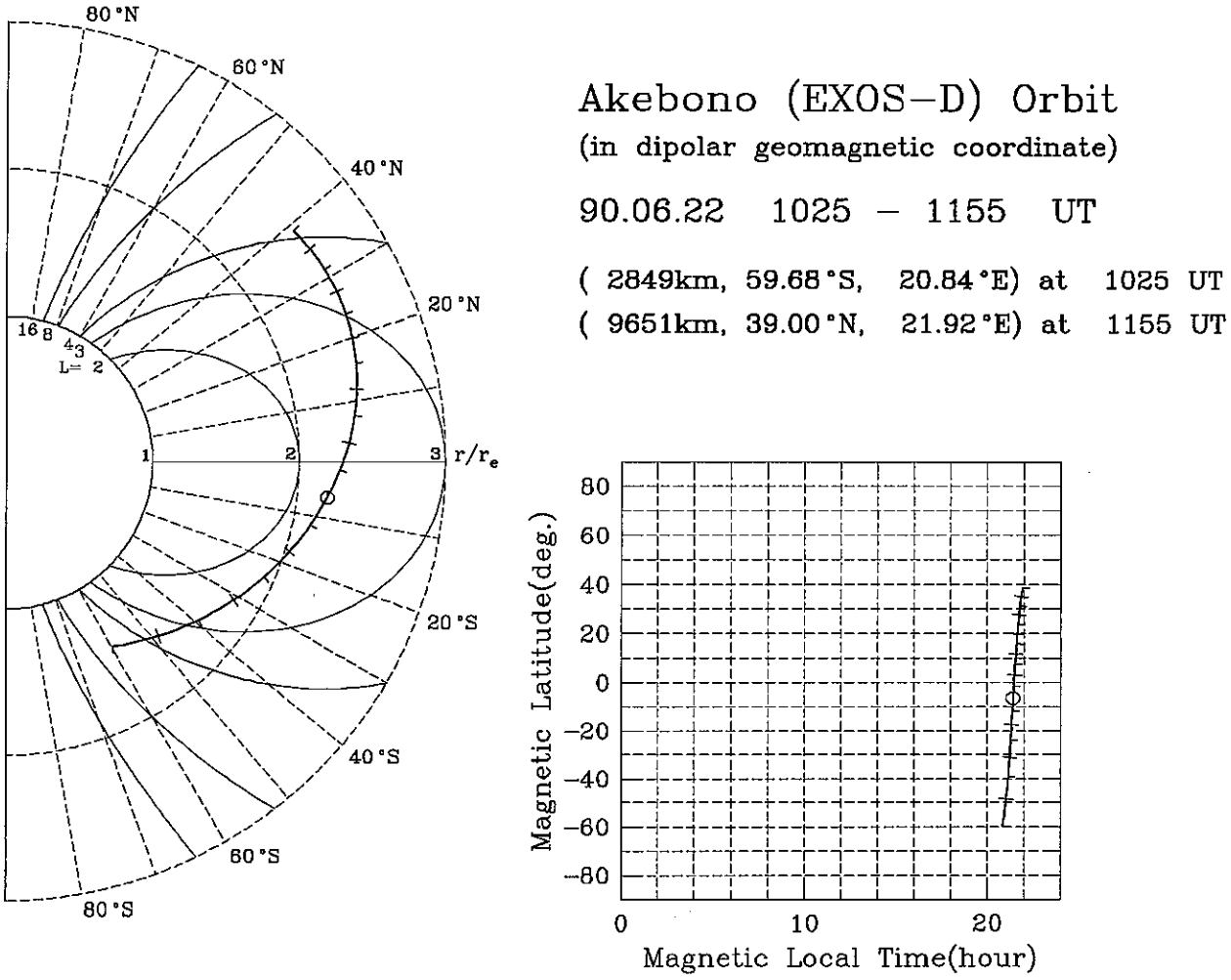

Figure 5. Akebono orbit from 1025 to 1155 UT on 22 June 1990.

25msec depending on the magnetic latitudes of the initial position of the ray tracing for Omega Australia, and 28msec–35msec for Omega Japan. The IRI model is considered to reflect an average figure for the electron density profile and the delay time derived from the IRI model are not strictly correct. The delay time itself is, however, at most, a few tens of milliseconds, except near the magnetic equator, and the error caused by using the IRI model is expected to be small.

2.3. Instruments Onboard the Akebono Satellite and Observational Data

[15] Omega signals were detected by the VLF (very low frequency plasma wave detectors) instrument [*Kimura et al.*, 1990] onboard the Akebono satellite. The Omega stations transmitted the common frequency 10.2kHz alternately with prescribed duration between 0.9 and 1.2sec at every 10sec. Since two electric and three magnetic field components of this frequency are observed onboard Akebono, we can determine the wave normal vectors of the received signals. In the direction finding analysis, we divided each duration of the Omega signals into four sections, and determined the wave normal directions for each section by the Means' method [*Means*, 1972]. We adopted the mean values of the wave normal directions whose variance is less than 20° for one duration. The delay time was defined as the time interval between the prescribed transmission time of the Omega signal and the risetime of the signal observed on Akebono.

[16] An example of the delay time and the wave normal directions determined by the above-mentioned procedure is shown in the left and right panels of Figure 3, respectively. In the abscissa of each panel, the universal time (UT), altitude (ALT), magnetic local time (MLT) and magnetic latitude (MLAT) are indicated. In

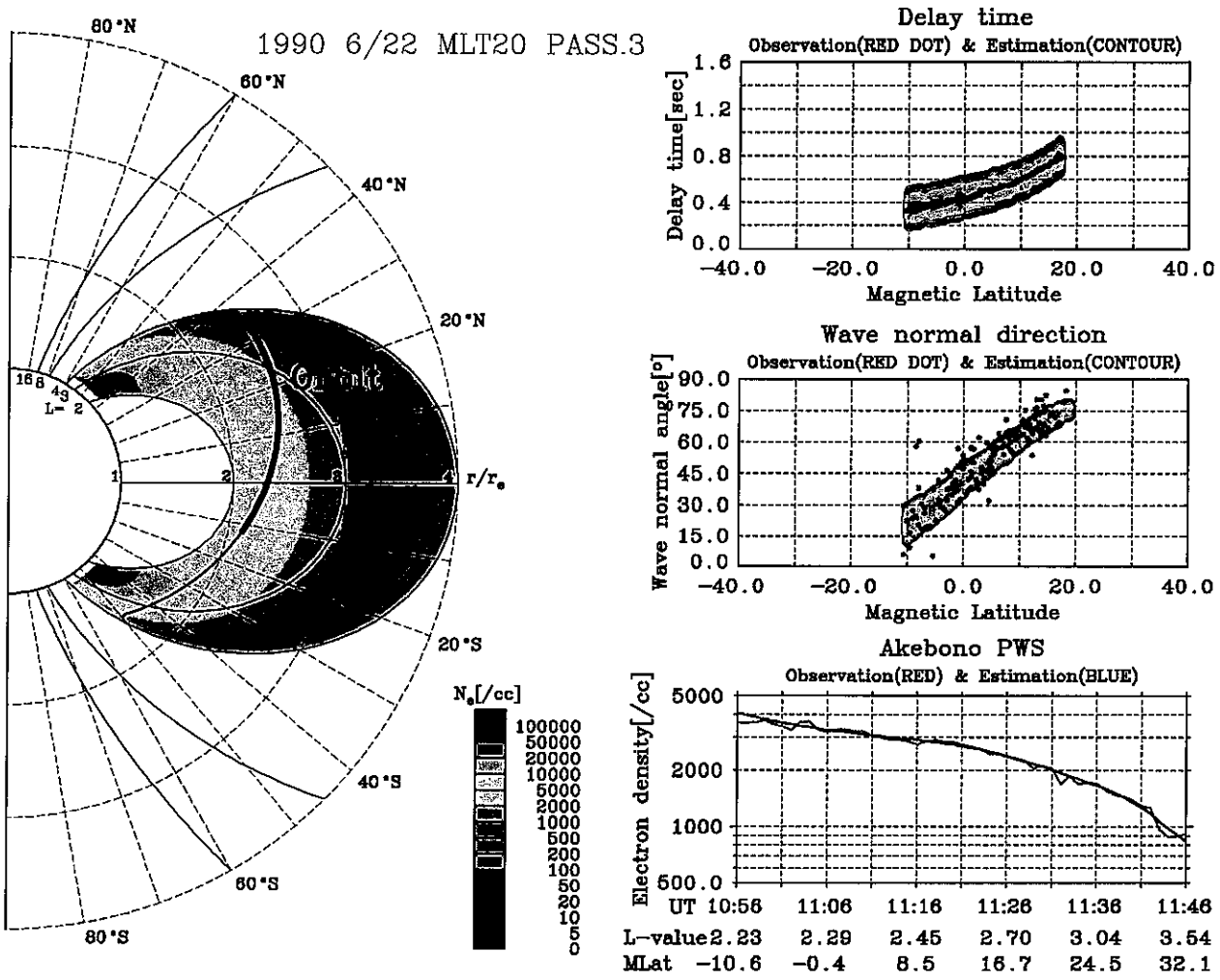

Figure 6. Global electron density contour map and fitting results on 22 June 1990. See color version of this figure at the back of this issue.

each panel of this figure, there appear to be two distinct groupings due to the source differences, that is, from the Australia station (circle) and the Japan station (box). Since Akebono moved northward in the plasmasphere during this period, the delay time of the Omega signals from Australia gradually increases, and that from Japan decreases.

[17] The electron density and temperature along the satellite trajectories are provided by the PWS (plasma wave observation and sounder experiment) instrument [*Oya et al.*, 1990] and the TED (temperature and energy distribution of plasma) instruments [*Abe et al.*, 1990] onboard Akebono, respectively. The accuracy of the obtained electron density is within 10%.

3. Application

3.1. Results of Analyses (1)

[18] In this section, we introduce electron density profiles reconstructed by the proposed method. Firstly, we apply the developed method to a series of observational data during the recovery phase of a magnetic storm. The *Dst* index during 11–24 June 1990 is shown in Figure 4, in which two sudden falls can be seen on the 13th and 14th. These falls signify magnetic storms. Figure 5 shows the trajectory of Akebono on 22 June 1990 (shown as (IV) in Figure 4). The Akebono was orbiting in the night side region around the magnetic local time of 20hr from the southern hemisphere to the

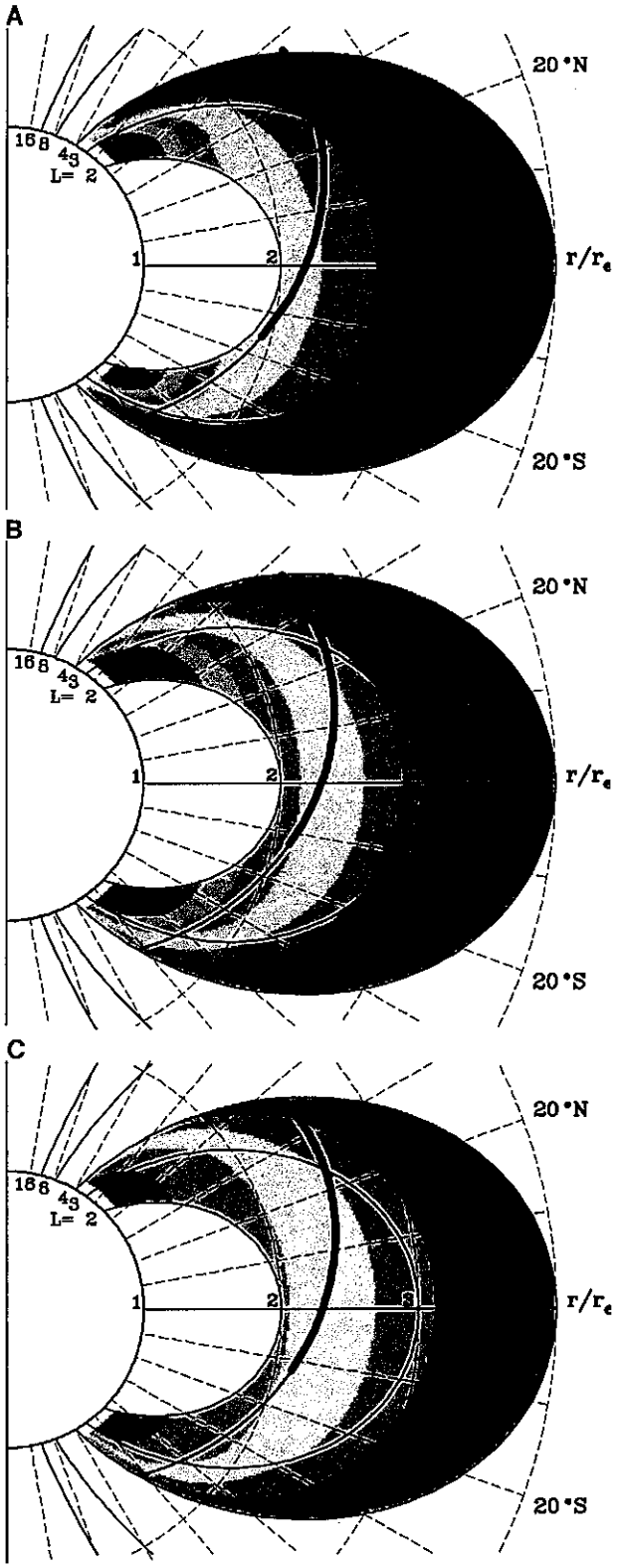

Figure 7. Variation of global density profile during the recovery phase of a magnetic storm. See color version of this figure at the back of this issue.

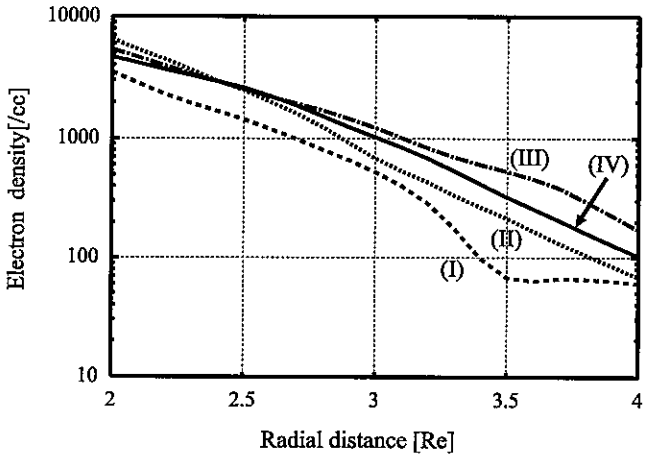

Figure 8. Electron density distribution along a radial line at the geomagnetic equator.

northern hemisphere. In this case, the Omega signals only from Australia were observed, and electron density data along the trajectory from 11°S to 32°N of the magnetic latitude were available.

[19] The observational data are shown in the right three panels in Figure 6. The delay time and the wave normal direction of the observed Omega signal are shown by red dots in the upper and middle panels, respectively. The abscissa in both indicate the magnetic latitude. The delay time and wave normal angle became larger as the satellite moved to higher latitudes in the northern hemisphere. In the lower panel, the observed electron density is shown by the red line. In the abscissa, the universal time (UT), L-value and magnetic latitude (MLAT) are indicated.

[20] The best fit theoretical PDFs of the delay time and the wave normal direction are shown by contour maps in each panel. The high probability of the PDF is represented by warm colors and low probability is by cold colors. From these figures, it is found that the observed delay time and wave normal angle correspond well with the theoretical PDFs. The reconstructed global electron density profile is represented by a contour map on the left side in Figure 6. The map shows the two-dimensional density profile in the meridian plane in the geomagnetic coordinate system. The solid line indicates the trajectory of the Akebono satellite and the thick black part shows the trajectory where the in situ electron density data were used. In the map, magnetic field lines are drawn along L-values of 2, 3, 4, 8 and 16. The estimated electron density along the satellite trajectory is shown by the blue line in the right lower panel in Figure 6. In this chart, small local fluctuations are successfully reduced.

[21] Three more cases ((I),(II) and (III) in Figure 4) were also examined during the recovery phase of the magnetic storm. In these cases, the trajectories of Akebono were almost the same as shown in Figure 5. Figure 7 shows the estimated density profiles for these cases. For all cases, the contour levels are the same as that of Figure 6, and the wave characteristics were also well fitted (not shown). At the beginning of the recovery phase (I), the high density region is compressed toward the Earth. After that, the distribution is gradually expanded, and it takes several days to reach a quiescent state. Figure 8 shows the electron density distributions along a radial line at the geomagnetic equator for each case. From the figure, the electron density at the geomagnetic equator on the 15th is found to be diminished to 70% at a radial distance of 2.0 and 20% at a radial distance of 3.5 compared with the quiescent state shown on the 20th and 22nd.

3.2. Results of Analyses (2)

[22] As another example, we demonstrate that the symmetry of the plasmaspheric density profile for the geomagnetic equator can be derived from two kinds of Omega signals propagating from northern and southern hemispheres using the developed method. Figure 9 shows the trajectory of Akebono on 4 July 1990. Akebono was passing from the southern to northern hemispheres around the magnetic local time of 20hr. There is little variation of the *Dst* index during this term, and it is considered to be in a quiescent state. In this example, we were able to obtain electron density data along the trajectory, both in the northern and southern hemispheres. In addition, the Omega signals from Australia and Japan were simultaneously observed along the trajectory, as shown in Figure 3. We estimate the electron density profiles using data sets of the two combinations shown in Table 1, respectively.

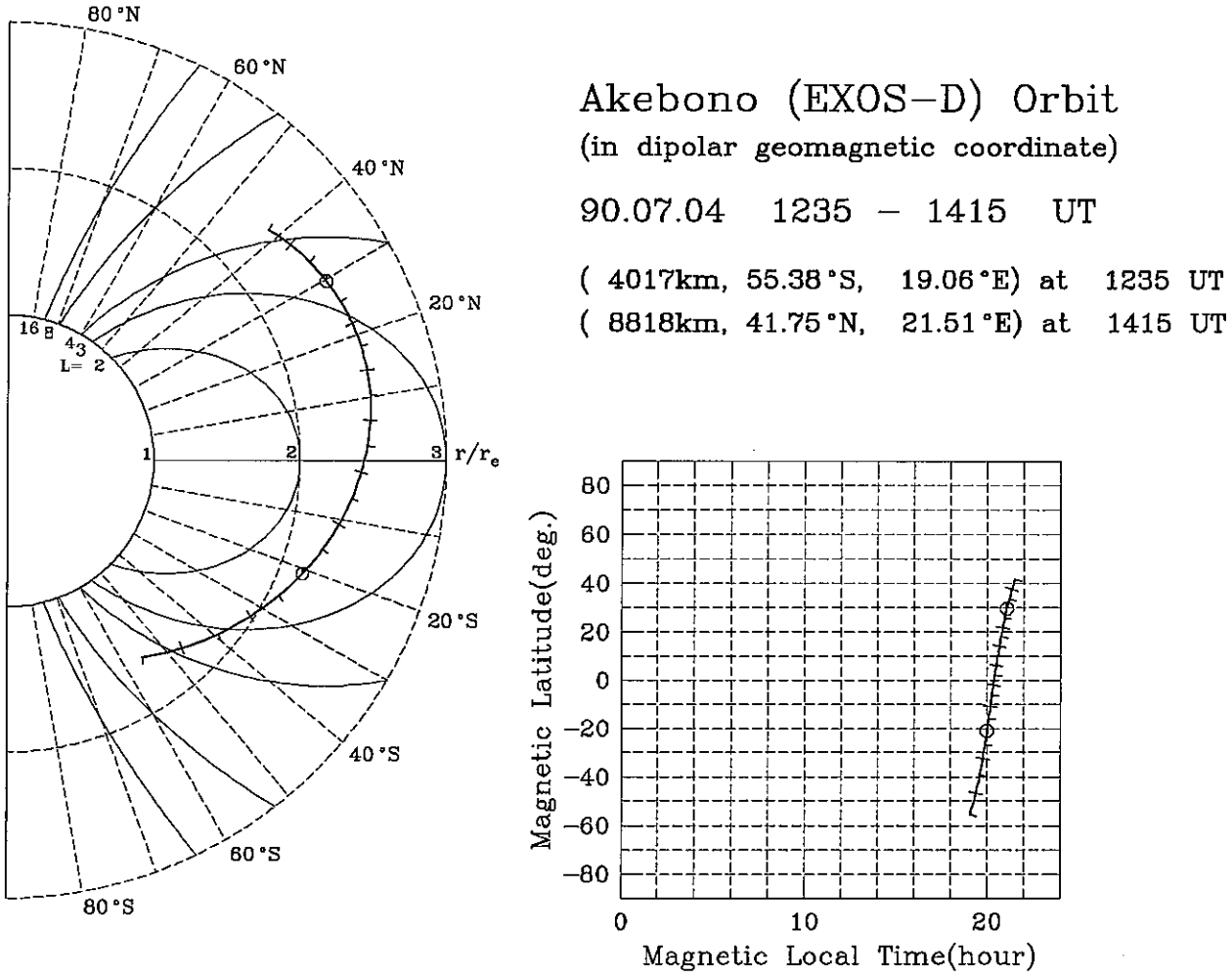

Figure 9. Akebono orbit from 1235 to 1415 UT on 4 July 1990.

[23] Although the density model is symmetric about the geomagnetic equator, the ray paths from the Omega station to the satellite mainly cover one hemisphere on the transmitter side. Therefore the estimated profile represents well half of the plasmasphere. Namely, the result of case (1) mainly reflects the density profile in the southern hemisphere, and in case (2), in the northern hemisphere.

Table 1. Data Sets: One for the Northern Hemisphere and One for the Southern Hemisphere

Electron Density	Omega Signal
Case (1) southern hemisphere (see Figure 10)	Australia
Case (2) northern hemisphere (see Figure 11)	Japan

[24] Figures 10 and 11 show the results of case (1) and case (2), respectively. Each panel display is the same as in the previous example. From the electron density along the trajectory shown in the right lower panel in Figure 10, it is found that the estimated density (blue) corresponds well to the observed (red) in the southern hemisphere but to a lesser extent in the northern hemisphere. In contrast, from Figure 11, the estimated density corresponds well to the observed in the northern hemisphere but is a little higher than in the southern hemisphere. We evaluate the differences in the estimated density profiles quantitively. The averaged relative difference between the northern and southern hemispheres at about 600 points distributed over a hemisphere is calculated. The difference amounts to about 15%.

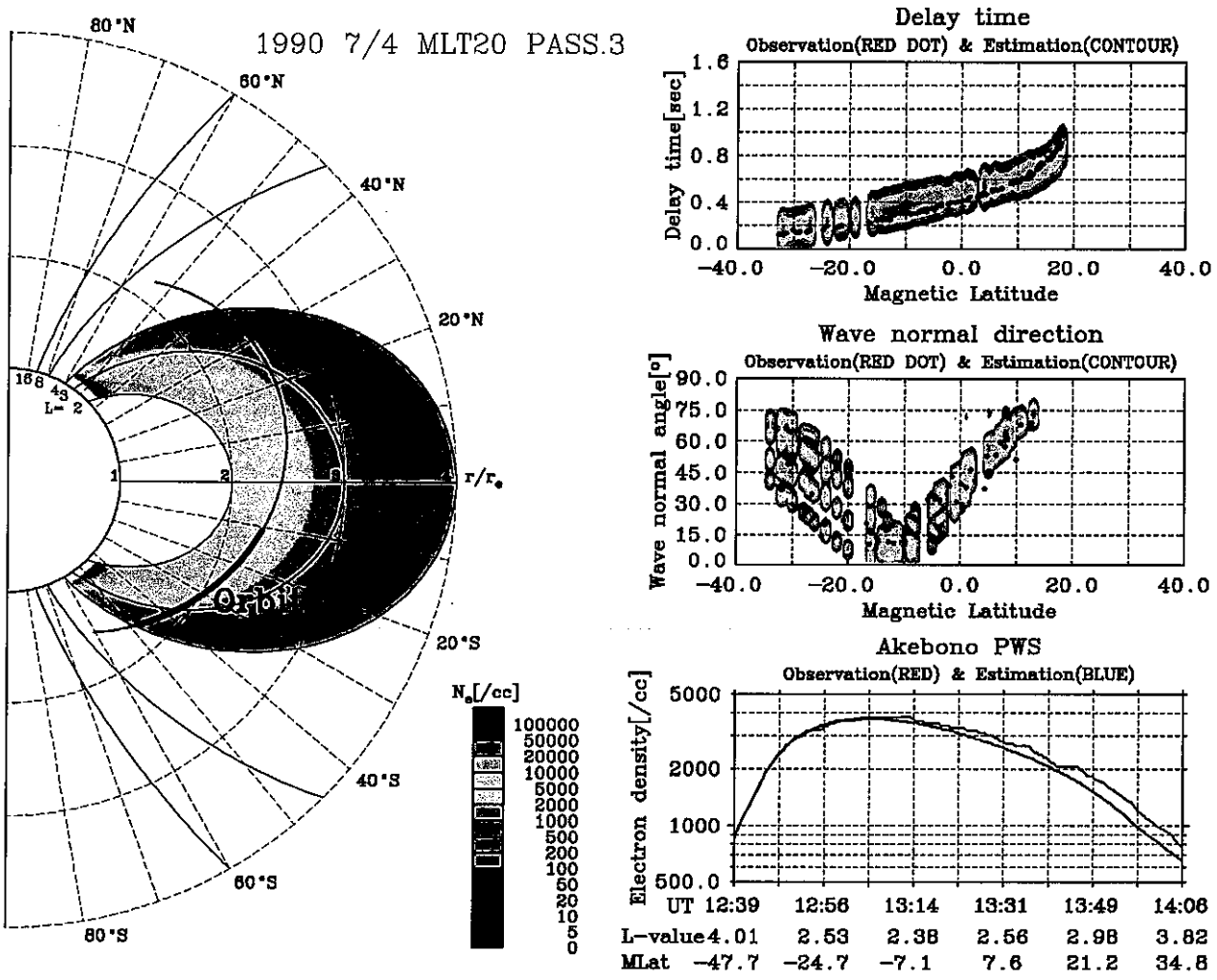

Figure 10. Global electron density map on 4 July 1990 derived from the southern hemisphere data and fitting results. See color version of this figure at the back of this issue.

4. Discussion

[25] We have shown several cases of global electron density profiles reconstructed by a developed method. In the first example, the variation of the global electron density profile during the recovery phase of a magnetic storm was examined. The results revealed clearly the global compression and refilling of the electron density profile. In the other example, we showed that the global electron density profile could be reconstructed separately in the northern and southern hemispheres using the two data sets, that is, one for the northern hemisphere and the other for the southern hemisphere.

[26] For each example, we verified that the observed wave normal directions and the delay times could not be reproduced well under other local minimum parameter sets and confirmed the uniqueness of the obtained solution. In addition, we also confirmed that the reconstructed profiles were invariant in the vicinity of the obtained solution where the ABIC is small enough to consider the wave normal directions and delay times calculated by ray tracing agree with the observed values. More realistic analytical models derived from recent satellite observations will improve the performance of the proposed method especially for complex conditions during storm-time and refilling.

[27] From the results using two data sets, we could not directly discuss the symmetry of the northern and southern hemispheres because the difference originated not only from the latitudinal asymmetry but also from the density variation due to corotation during the obser-

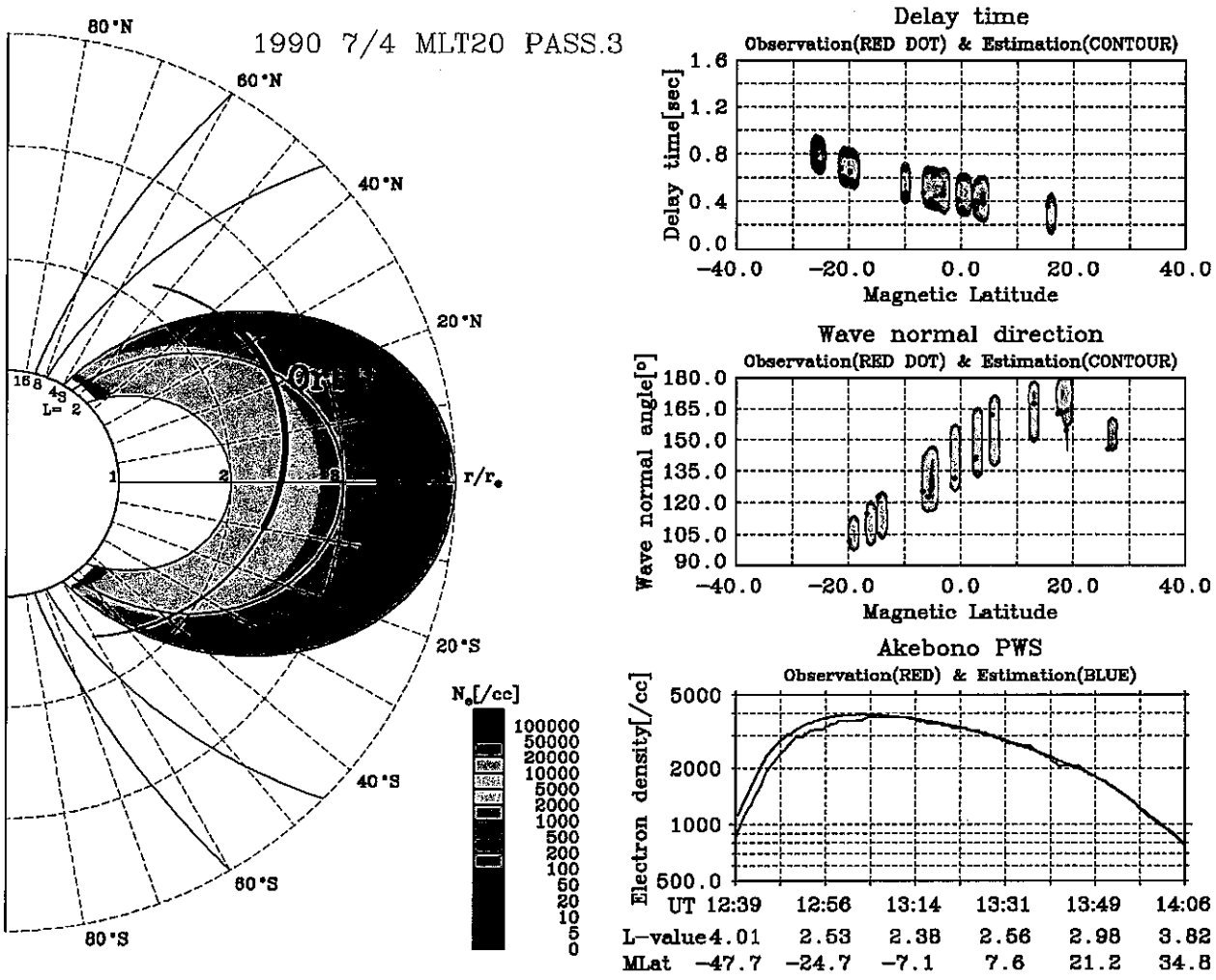

Figure 11. Global electron density map on 4 July 1990 derived from the northern hemisphere data and fitting results. See color version of this figure at the back of this issue.

vation period. We tested the proposed method for sensitibity to north-south differences using simulated data for the cases; "azimuthally stationary and latitudinally asymmetric profiles," and "azimuthally unstationary and latitudinally symmetric profiles." In each case, we confirmed that the the degree of the north-south differences in the original data was correctly estimated when the density profile had either latitudinal asymmetry or azimuthally unstationary structure. This result implies that the latitudinal asymmetry derived in the case of 3.2 is on the order of 15% at most, which is less than the uncertainty of the estimate. This way, the proposed method can detect north-south differences to some extent. In the case, where considerable north-south differences are detected, it is necessary to discriminate between latitudinal asymmetry and the density variation due to corotation during the observation period using other methods.

5. Conclusions

[28] In the present paper, we introduced a flexible plasmaspheric density model and a fitting algorithm, in which stochastic factors are taken into account. In order to separate the effects of the ionosphere and the plasmasphere, ray tracing was initiated from an altitude of 500km, giving adequate initial values. The delay time in the ionosphere was calculated from the integral of the square root of the IRI-derived electron density profile along the ray path. For the wave normal direction, we took various possibilities into account at an altitude of 500km and gave all of them the initial values of the ray tracing.

[29] We examined the validity of the proposed method by applying it to the observational data during a magnetic storm. From the result, it was found that density profiles which are consistent with the VLF wave propagations could be reconstructed with the proposed model. In the other example, we estimated the density profiles in the northern and southern hemispheres independently, and demonstrated that the symmetry of the plasmaspheric density profile for the geomagnetic equator could be derived using the proposed method.

[30] **Acknowledgments.** We thank H. Oya for providing the electron density data observed by Akebono. We also thank T. Abe for providing us with the electron temperature data observed by Akebono through DARTS at the Institute of Space and Astronautical Science (ISAS) in Japan. We wish to express our deep appreciation to I. Kimura for his comments throughout the present work. We also wish to express our deep appreciation to T. Higuchi for his constructive suggestions. We are also grateful to the Akebono/VLF members for their contribution of the VLF instrument and its data analyses. The *Dst* index data were provided from World Data Center for Geomagnetism, Kyoto.

References

Abe, T., K. Oyama, H. Amemiya, S. Watanabe, H. Mori, and E. Sagawa, Measurements of temperature and velocity distribution of thermal electrons by the Akebono (EXOS-D) satellite–Experimental setup and preliminary results, *J. Geomagn. Geoelectr.*, *42*, 537–554, 1990.

Akaike, H., Likelihood and the Bayes procedure, in *Bayesian Statistics*, edited by J. M. Bernardo et al., pp. 143–166, Univ. Press, Valencia, Spain, 1980.

Angerami, J. J., and J. O. Thomas, Studies of planetary atmospheres: 1. The distribution of ions and electrons in the Earth's exosphere, *J. Geophys. Res.*, *69*, 4537–4560, 1964.

Bailey, G. J., N. Balan, and Y. Z. Su, The Sheffield University plasmasphere ionosphere model—A review., *J. Atoms. Terr. Phys.*, *59*, 1541–1552, 1996.

Bilitza, D., K. Rawer, L. Bossy, and T. Gulyaeva, International reference ionosphere—Past, present, future, *Adv. Space. Res.*, *13*(3), 3–23, 1993.

Cummer, S. A., M. J. Reiner, B. W. Reinisch, M. L. Kaiser, J. L. Green, R. F. Benson, R. Manning, and K. Goetz, A test of magnetospheric radio tomographic imaging with IMAGE and WIND, *Geophys. Res. Lett.*, *28*, 1131–1134, 2001.

Davies, K., and G. K. Hartmann, Studying the ionosphere with the global positioning system, *Radio Sci.*, *32*, 1695–1703, 1997.

Ergun, R. E., et al., Feasibility of a multisatellite investigation of the Earth's magnetosphere with radio tomography, *J. Geophys. Res.*, *105*, 361–373, 2000.

Ganguly, A., G. H. Van Bavel, and A. Brown, Imaging electron density and magnetic field distributions in the magnetosphere: A new technique, *J. Geophys. Res.*, *105*, 16,063–16,081, 2000.

Goto, Y., Y. Kasahara, and T. Sato, A flexible modeling of global plasma profile deduced from wave data, in *Progress in Discovery Science, Lecture Notes in Computer Science*, vol. 2281, edited by S., Arikawa and A. Shinohara, pp. 438–448, Springer-Verlag, New York, 2002.

Kimura, I., K. Hashimoto, I. Nagano, T. Okada, M. Yamamoto, T. Yoshino, H. Matsumoto, M. Ejiri, and K. Hayashi, VLF observations by the Akebono (EXOS-D) satellite, *J. Geomagn. Geoelectr.*, *42*, 459–478, 1990.

Kimura, I., A. Hikuma, Y. Kasahara, and H. Oya, Electron density distribution in the plasmasphere in conjunction with IRI model, deduced from Akebono wave data, *Adv. Space. Res.*, *18*(6), 279–288, 1996.

Kimura, I., K. Tsunehara, A. Hikuma, Y. Z. Su, Y. Kasahara, and H. Oya, Global electron density distribution in the plasmasphere deduced from Akebono wave data and the IRI model, *J. Atoms. Terr. Phys.*, *59*, 1569–1586, 1997.

Kimura, I., Y. Kasahara, and H. Oya, Determination of global plasmaspheric electron density profile by tomographic approach using Omega signals and ray tracing, *J. Atoms. Terr. Phys.*, *63*, 1157–1170, 2001.

Mannucci, A. J., B. D. Wilson, D. N. Yuan, C. H. Ho, U. J. Lindqwister, and T. F. Runge, A global mapping technique for GPS-derived ionospheric total electron content measurements, *Radio Sci.*, *33*, 565–582, 1998.

Means, J. D., Use of three-dimensional covariance matrix in analyzing the properties of plane waves, *J. Geophys. Res.*, *77*, 5551–5559, 1972.

Oya, H., A. Morioka, K. Kobayashi, M. Iizima, T. Ono, H. Miyaoka, T. Okada, and T. Obara, Plasma Wave Observation and Sounder Experiments (PWS) using the Akebono (EXOS-D) satellite—Instrumentation and initial results including discovery of the high altitude equatorial plasma turbulence, *J. Geomagn. Geoelectr.*, *42*, 411–442, 1990.

Reinisch, B. W., et al., First results from the Radio Plasma Imager on IMAGE, *Geophys. Res. Lett.*, *28*, 1167–1170, 2001.

Scarabucci, R. R., Interpretation of VLF signals observed on the OGO-4 satellite, *Stanford Univ. Tech. Rep. 3418-2*, Stanford Radio Sci. Lab., Stanford, Calif., 1969.

Strangeways, J. H., A model for the electron temperature variation along geomagnetic field lines and its effect on electron density profiles and VLF ray paths, *J. Atmos. Terr. Phys.*, *48*, 671–683, 1986.

Y. Goto and T. Sato, Department of Communications and Computer Engineering, Kyoto University, Yoshida, Sakyo-ku, 606-8501 Kyoto, Japan. (ygotou@aso.cce.i.kyoto-u.ac.jp)

Y. Kasahara, Department of Information and Systems Engineering, Kanazawa University, 920-8667 Kanazawa, Japan.

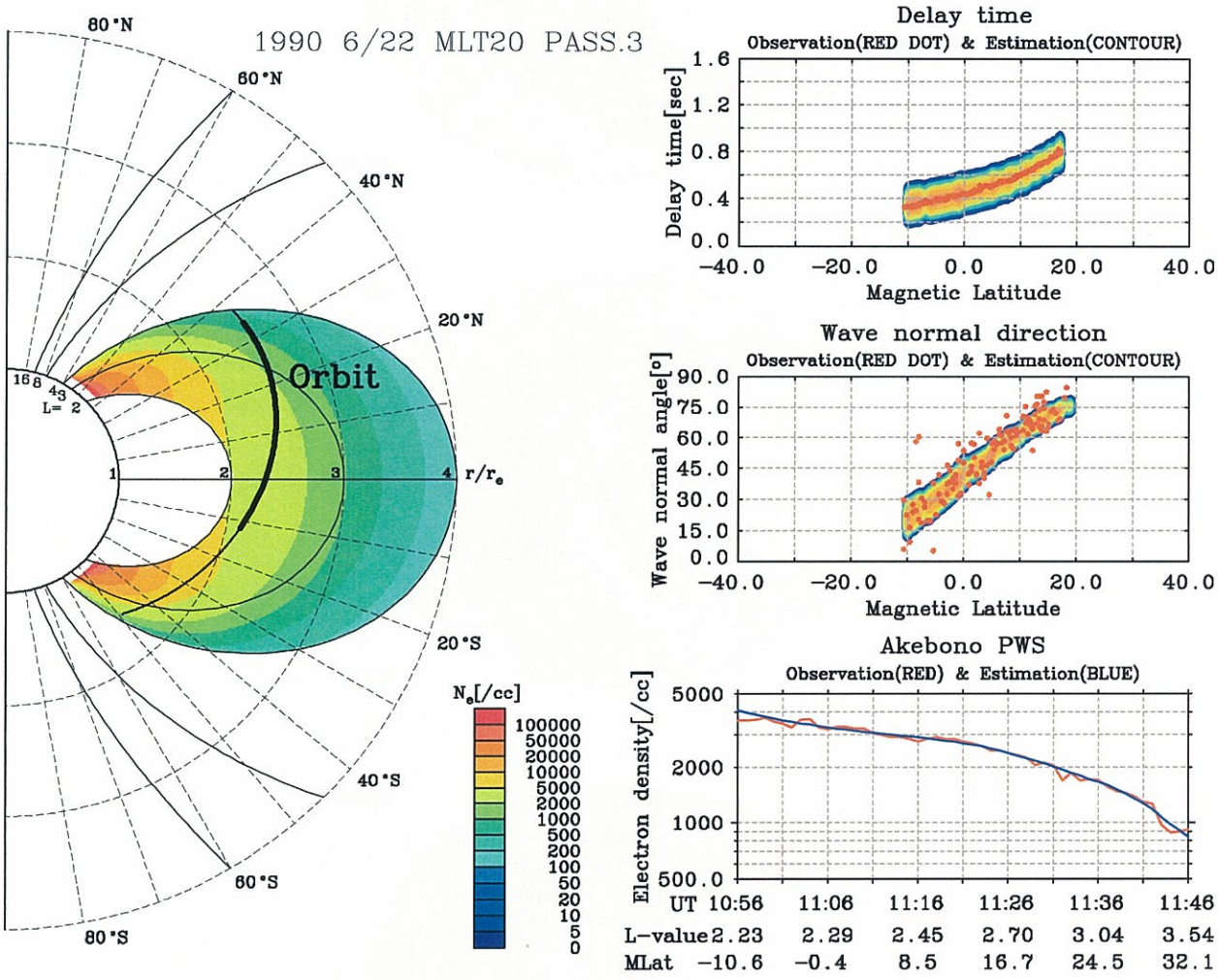

Figure 6. Global electron density contour map and fitting results on 22 June 1990.

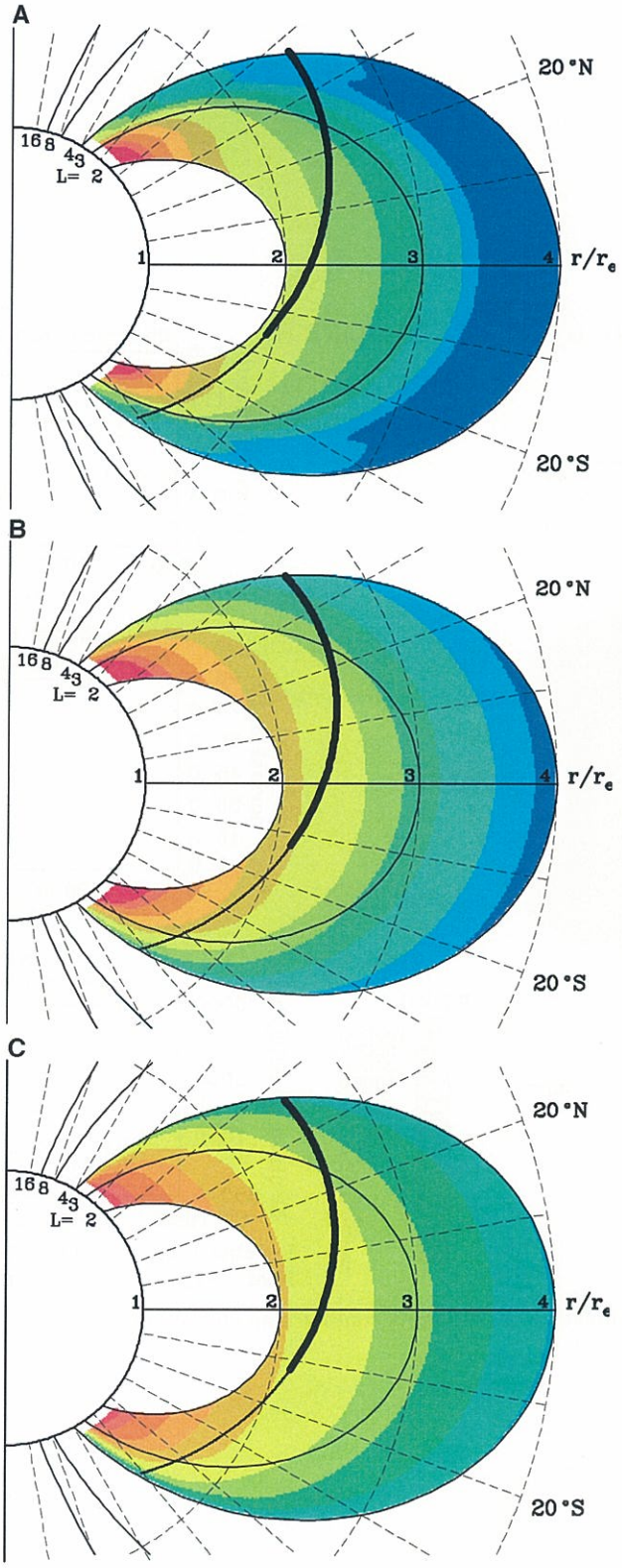

Figure 7. Variation of global density profile during the recovery phase of a magnetic storm

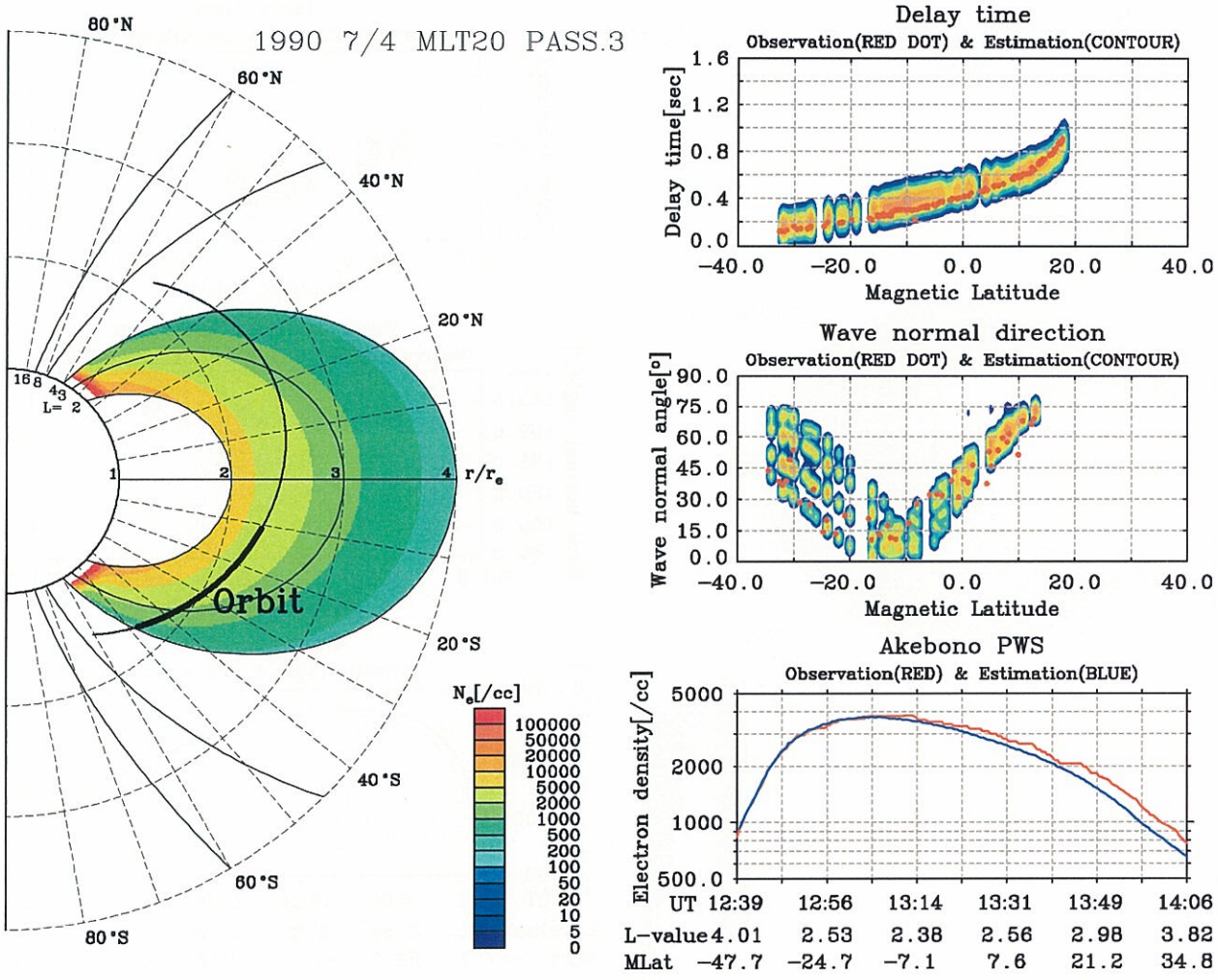

Figure 10. Global electron density map on 4 July 1990 derived from the southern hemisphere data and fitting results.

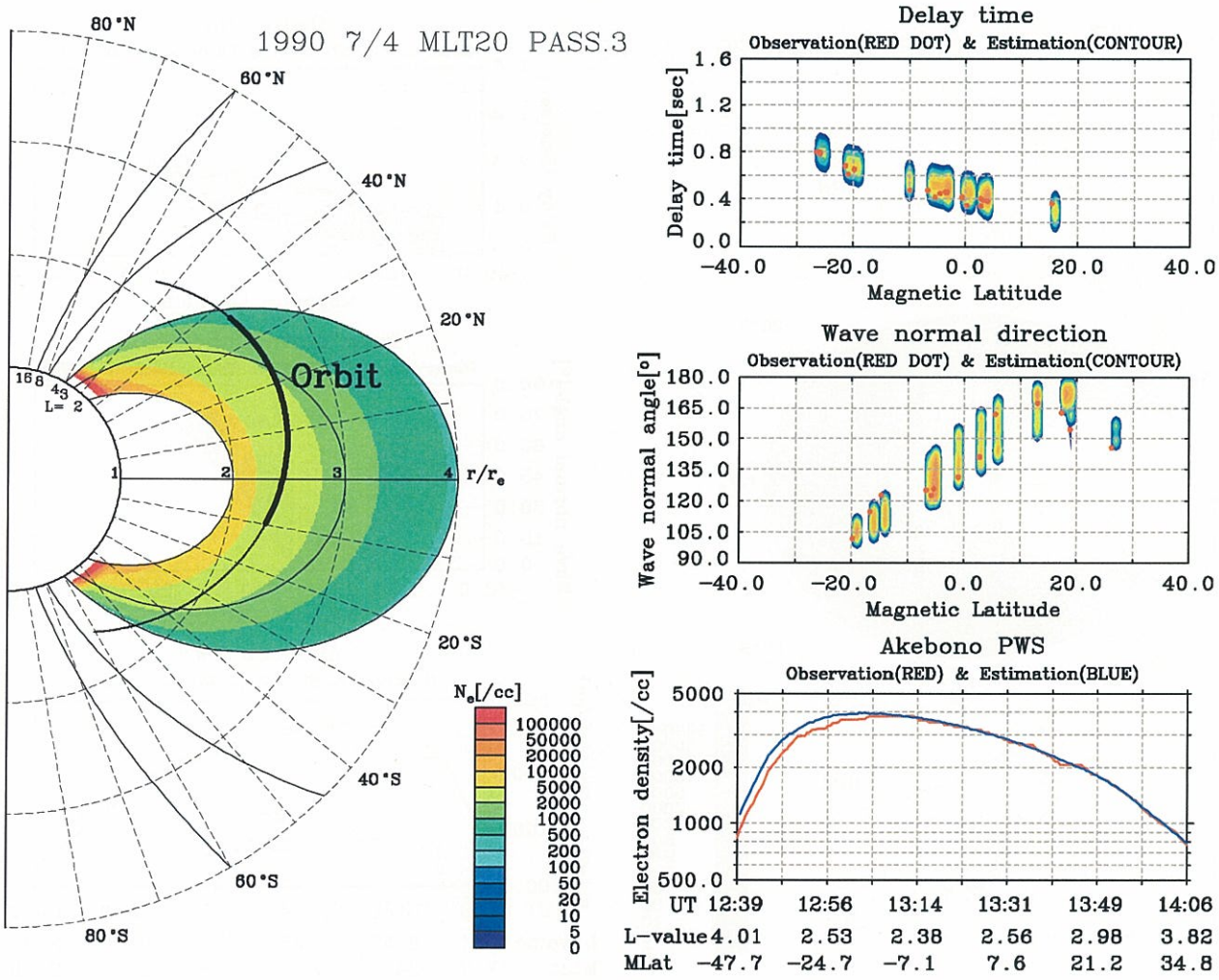

Figure 11. Global electron density map on 4 July 1990 derived from the northern hemisphere data and fitting results.